Raman Study on the G Mode of Graphene for Determination of Edge Orientation

Chunxiao Cong, Ting Yu,* and Haomin Wang

Division of Physics and Applied Physics, School of Physical and Mathematical Sciences, Nanyang Technological University, Singapore 637371

ARTICLE

ABSTRACT We report a confocal Raman study on edges of single-layer graphene. It is found that edge orientations could be identified by G mode in addition to D mode. We observe that G mode at the edges of single-layer graphene exhibits polar behaviors and different edges such as zigzag- or armchair-dominated responses differently than the polarization of the incident laser. Moreover, G mode shows stiffening at zigzag-dominated edges, while it is softened at armchair-dominated ones. Our observations are in good agreement with recent theory (Sasaki, K. *et al. J. Phys. Soc. Jpn.* 2010, *79*, 044603) and could be well-explained by the unique properties of pseudospin at graphene edges, which lead to asymmetry of Raman active modes and non-adiabatic processes (Kohn Anomaly) at different types of edges. This work could be useful for further study on the properties of the graphene edge and development of graphene-based devices.

KEYWORDS: graphene · edge orientation · Raman · polarization

Graphene, the mother material of other sp^2 carbon allotropes, became the most shining star in the carbon family since it was discovered experimentally and its quantum Hall properties were reported.[1−3] Among the research interests of graphene, the edge is one of the focuses because physical properties of graphene, especially graphene nanoribbons, are mainly determined by edges. Some edges with certain symmetry may have localized edge states while others do not.[4,5] The superconductivity,[6] ferromagnetism,[4] and exceptional quantum Hall effect[7] might be a result from these localized edge states. Different types of edges may also have various favorites to functional chemical and biological groups, which could certainly extend the potentials of graphene.[8]

Raman spectroscopy is a unique and one of the most powerful techniques for graphene studies. Usually, two strong peaks are presented in the Raman spectrum of graphene of large dimension and high quality, named G and G′ (or 2D) modes. If the laser beam is focused on the edges of graphene or some defects exist, another peak will appear, called the D mode. All Raman modes of graphene are resonant, meaning phonons represented by these modes strongly interact with electrons and holes through the famous single resonance for G mode and intervalley double resonance for D and G′ modes.[9] An elastic scattering by defects is required for observation of the D mode.[10] Thus, by monitoring the position, width, integrated intensity, and so on, the number of layers,[11,12] linear dispersion of electronic energy,[13] crystal orientation,[14,15] doping,[16,17] defects,[18] and strain[19,20] could be probed by Raman study. Most recently, we demonstrated that the armchair-dominated edge could be distinguished from the zigzag-dominated edge by reading the integrated intensity of the D mode. This could be well-explained by the defect-assisted double resonant intervalley scattering process.[21,22]

In this paper, we demonstrate the orientation identification of the graphene edge through the G mode. In contrast to the body of the graphene sheet, the G mode at the edge exhibits obvious polarization dependence. The opposite polar behaviors of the armchair edge (*A*-edge) and zigzag edge (*Z*-edge) could be an alternative way to effectively identify the orientation of graphene edges. In addition, the presence and removal of non-adiabatic Kohn anomaly have also been seen at *A*- and *Z*-edges, respectively, which is also an option for determining edge orientation.

RESULTS AND DISCUSSION

Considering the crystal nature of graphene, only SLG sheets having edges with a relative angle of a multiple of 30° were selected. As shown in Figure 1A, a 90° corner between two adjacent edges can be

*Address correspondence to yuting@ntu.edu.sg.

Received for review April 7, 2010 and accepted April 30, 2010.

Published online May 6, 2010.
10.1021/nn100705n

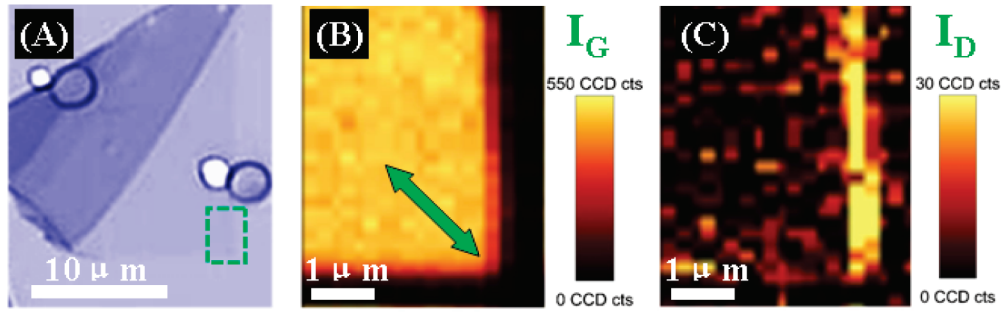

Figure 1. (A) Optical image of SLG with two edges at 90°. (B,C) Raman images of the interested area highlighted in (A) by extracting the integrated intensity of G and D modes, respectively. The polarization of the incident laser is at 45° to each of the edges as illustrated.

clearly seen in the optical image. Two peaks, named G and G′ modes, are observed when the laser beam was focused on the body of the SLG sheet (inset of Figure S1A in Supporting Information). By extracting the integrated intensity of the G mode, a Raman image of the corner of interest is constructed (Figure 1B) and exhibits a significant contrast between the main body and edges, indicating a dramatic decrease of G mode intensity moving from inside to outside. The profile of the G mode intensity across the edges reveals step-function dependence, as shown in Figure S1A, which agrees well with a previous report.[23] Differing from G mode, D mode originating from a defect-assisted double resonance process localizes at one edge (Figure 1C) when the polarization of the incident laser is tuned to 45° with respect to each of the edges. The localization of the D mode could be well-demonstrated by the Gaussian profile (Figure S1B). The strong D mode at the vertical edge and very weak D mode at the horizontal edge suggest the *A*- and *Z*-edge nature of the edges, respectively, because the *A*-edge could scatter electrons from one to the other valley near the Dirac points—so-called intervalley scattering—whereas the *Z*-edge cannot.[22] Hereinafter, we label the vertical edge as armchair and the horizontal as zigzag.

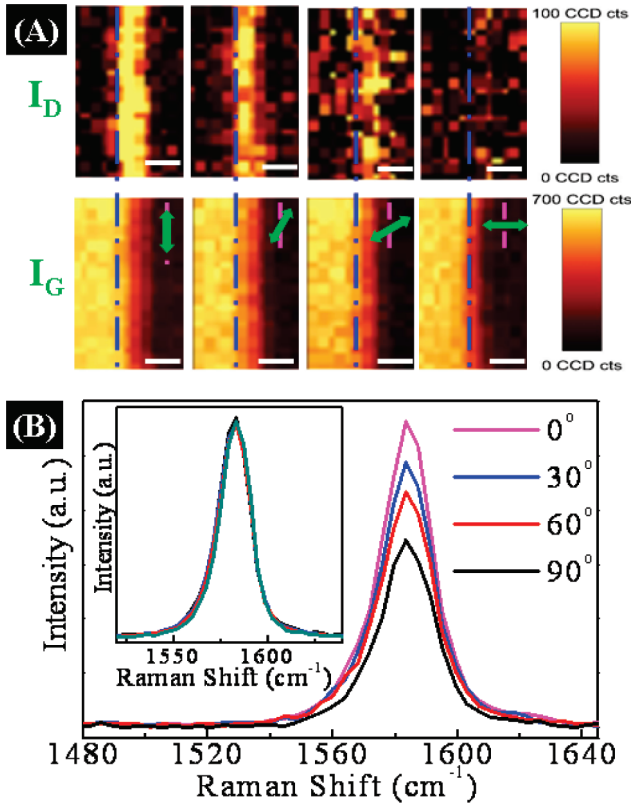

Figure 2. (A) Raman images of D (top) and G (bottom) intensities. The polarization of the incident laser is tuned to be 0, 30, 60, and 90° with respect to the armchair edge (scale bar is 400 nm). (B) Typical Raman spectra of the armchair edge showing the polarization dependence of the G mode. The inset plots the corresponding Raman spectra taken from the body.

Considering the fact that the width of the edge for the G mode is very narrow as a consequence of zero momentum of such G phonons,[24] and to effectively collect enough signal from the edge, polarization-dependent Raman mapping of the G mode is conducted. As shown in the bottom of Figure 2A, with increasing the angles of the incident electric field relative to the *A*-edge, the G modes become weaker and minimum at 90°, which is consistent with theoretical results.[25] In comparison, the polar behavior of the D mode is also revealed by a group of polar Raman images shown in the top of Figure 2A. It can be clearly seen that the intensity of the D mode decreases with the increase of the angles. As known, the intensity of the D mode is proportional to [**e** × **p**], where **e** is the polarization of the incident laser, and **p** is the momentum of the photoexcited electron or hole relative to the Dirac point. As such, the strongest D mode appears when the polarization of the incident light is parallel to the *A*-edge. Essentially, the intensity of the D mode follows $I_D \propto \cos^2(\theta_{in})\cos^2(\theta_{out})$, where θ_{in} and θ_{out} represent the angles of the incident and scattering electric fields relative to the edge, respectively.[23,24] In this work, we did not put an analyzer in the scattering beam. Therefore, the intensity of the D mode is only proportional to $\cos^2(\theta_{in})$, as shown in Figure S2 (Supporting Information). A ratio of 0.2 between the I_{Dmin} to I_{Dmax} is obtained, implying a high purity and degree of order of this *A*-edge.[24] Figure 2B shows the typical Raman spectra of the G mode at the *A*-edge with various polar angles. The inset plots the corresponding Raman spectra taken from the body. This polarization independence directly

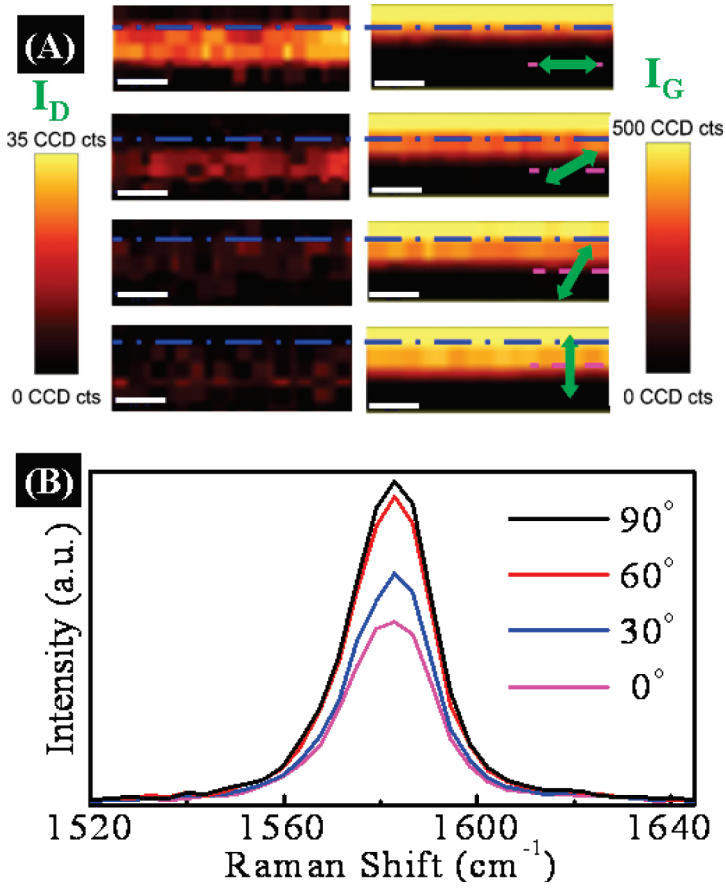

Figure 3. (A) Raman images of D (left) and G (right) intensities. The polarization of the incident laser is tuned to be 0, 30, 60, and 90° with respect to the average direction of the zigzag edge (scale bar is 400 nm). (B) Typical Raman spectra of the zigzag edge showing the polarization dependence of the G mode.

results from the nature of the G mode in graphene, which has an E_{2g} symmetry (space group $P6_3/mmc$),[26] and the two doubly degenerate Raman polarizability tensors function by reflecting the polarization vector about the $x = y$ and $y = 0$ with identical scattering efficiency.[14,23,27]

Figure 3 shows the polarization dependence of both G and D modes at the *Z*-edge. Obviously, the polar behavior of the G mode at the *Z*-edge differs strongly from that at the *A*-edge. The larger polar angles lead to stronger G mode at the *Z*-edge as predicted by the theoretical work.[25] Weak D mode caused by the existence of some armchair segments at the *Z*-edge still obeys the standard dependence. The typical Raman spectra of the G mode at the zigzag edge are shown in Figure 3B.

To further elucidate the polarization dependence of the G mode at both *A*- and *Z*-edges, the intensities of the G mode are plotted as a function of polar angles, as shown in Figure 4. Since the G mode at the main body has no polarization dependence, the data were normalized to the I_G at the body. For the *A*-edge (Figure 4A), $\cos^2(\theta_{in})$ is employed to fit the experimental data, whereas the intensity of the G mode at the *Z*-edge (Fig-

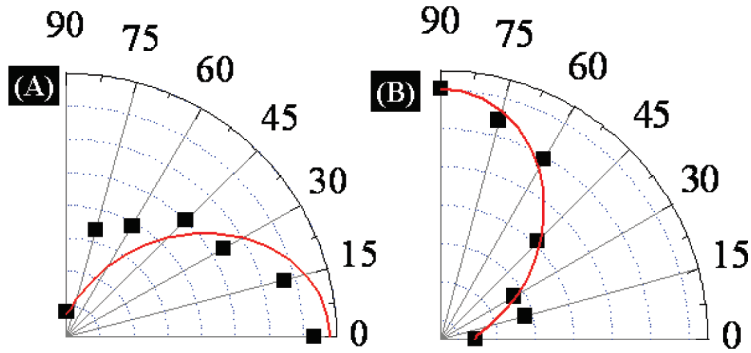

Figure 4. Polar plots of the integrated intensity of the G mode at the (A) *A*-edge and (B) *Z*-edge. The red solid line is the fitting curve of (A) $I_G \propto \cos^2(\theta_{in})$ and (B) $I_G \propto \sin^2(\theta_{in})$ of the experimental data.

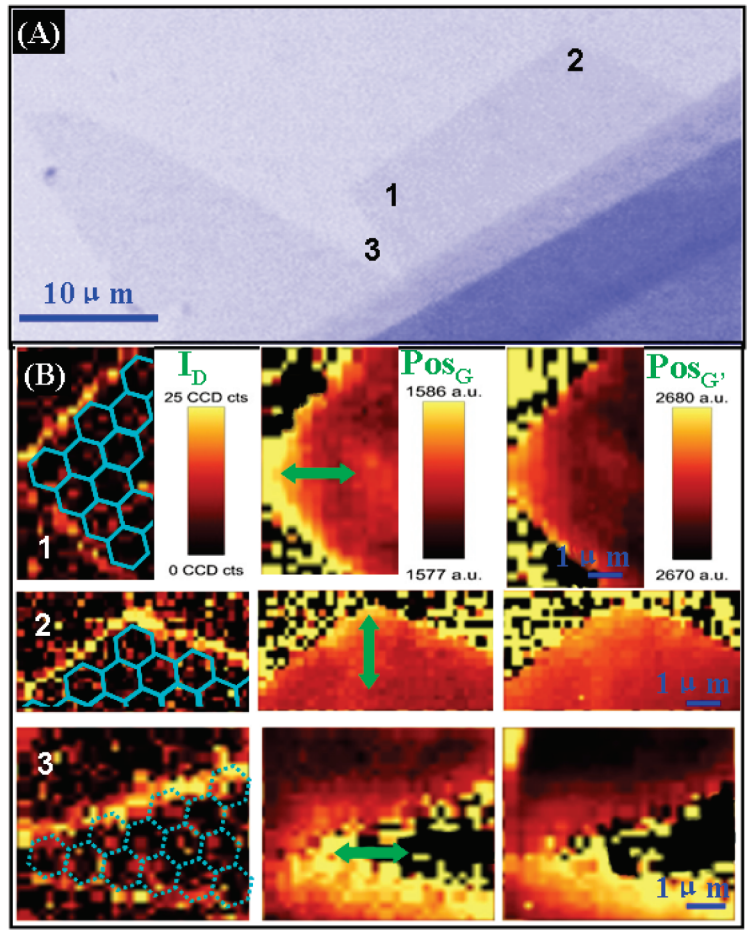

Figure 5. (A) Optical image of SLG with a 90, 120, and 330° corner labeled as 1, 2, and 3, respectively. (B) Raman images of the integrated intensity of the D mode (left), position of the G mode (middle), and position of the G′ mode (right), respectively.

ure 4B) follows $\sin^2(\theta_{in})$ perfectly. The appearance of remarkable polar behavior at the edges differs sharply from that at the body. This is because the two degenerate components of the G mode, longitudinal optical (LO) and transverse optical (TO) phonons, no longer participate in the scattering process equally. In fact, only the LO mode is active at the armchair edge while the TO mode is dominant at the zigzag edge.[25]

Figure 5A is an optical image of a SLG sheet with a 90° (labeled as 1), 120° (labeled as 2), and 330° (labeled as 3) corner. Figure 5B (left) shows the Raman mapping of the D mode of these three corners. As expected, at 90 and 330° corners, one edge presents stronger D mode while the other exhibits a weaker one, whereas the two edges with an angle of 120° show almost the same contrast. On the basis of the previous analysis, the edge orientations are identified, as illustrated in Figure 5B (left). Interestingly, when we plotted the images of the G mode to show the distribution of the G peak position over the corners (Figure 5B, middle), we noticed that the zigzag edges appear brighter compared to the other part, meaning that a blue shift occurs to the G mode at the zigzag edges. Two mechanisms could be responsible for such a blue shift for the zigzag edge or relatively a red shift for the armchair edge and main body. One is uniaxial strain, and the other is Kohn anomaly. Tensile (compressive) strain is able to lower (increase) the frequency of G phonons (both LO and TO components).[28] In addition to the G mode, strain could also cause the shift of the G′ mode, and actually, the G′ mode is more sensitive to the strain.[20] So, we examined the G′ mode by the Raman mapping of the G′ mode position (Figure 5B, right). Among three images, only the 330° corner shows an obvious blue shift at the *Z*-edge, which is coincident with the G mode and implies that the strain might be one of the reasons resulting in such a blue shift at this edge. Since the images of the 90 and 120° corners present quite uniform distribution of the position of the G′ mode over the entire area, we should consider the other possible process causing such a difference of G peak position—Kohn anomaly—a process capable of softening Γ point phonons (G mode in graphene) with a zero momentum through a phonon−electron interaction.[29] Due to the unique crystal configurations at the *A*- and *Z*-edges, the TO phonons at both zigzag and armchair have almost no contribution to the creation of an electron−hole, a critical step in the Kohn anomaly,

which means that the TO mode cannot undergo the Kohn anomaly as a contrast to the LO mode.[29] Previous analyses have revealed that the LO mode is only active at the *A*-edge. Hence, the Kohn anomaly is expected to happen to the G mode at the *A*-edge and lead to a red shift of the G mode as we observed (Figure 5B, middle). The relative blue shift of the G mode at the *Z*-edge is the consequence of breaking Kohn anomaly because the LO mode is not active at the *Z*-edge.

In summary, we studied the G mode at the edges of SLG sheets by Raman spectroscopy and mapping. Different polarization dependence of the G mode at *Z*- and *A*-edges (predetermined by the D mode) has been observed and could be well-explained by the unequal interaction between LO and TO phonons with electrons at the different types of edges. Kohn anomaly at the *A*-edge and breaking of Kohn anomaly at the *Z*-edge have been demonstrated by the Raman mapping of the G mode position. Further studies on this Kohn anomaly at the edge of graphene are needed as we did observe the coincidence of blue shift of both G and G′ modes, a likely result of strain effect.

EXPERIMENTAL METHODS

Graphene samples were prepared by micromechanical cleavage of natural graphite crystals and transferred on a Si wafer with 300 nm oxide cap layer. Single-layer graphene (SLG) flakes were selected by reading the width of the G′ mode.[11] Raman spectra and images were obtained by a WITeck CRM200 confocal microscopy Raman system with a piezocrystal controlled scanning stage. The excitation light is a 532 nm laser. The laser spot size is estimated to be 500 nm. To avoid damaging and heating, the laser was attenuated and the power was controlled below 2 mW. The fast scan rate of 1 s per pixel also helped to minimize the laser effects. The polarization of the incident laser was tuned by rotating a half-wave plate.

Supporting Information Available: Ten samples have been examined in total. Seven samples clearly show contrast of D mode intensity between two adjacent edges, and 3 samples among these 7 present different polarization dependence of G mode and/or Kohn anomaly. The relatively low frequency of observing G mode polar behavior and Kohn anomaly could be due to the fact that edges of graphene are more sensitive to other factors such as strain and doping, which could effectively change the G mode position and intensity. Furthermore, the effective edge for G mode is very narrow, and the G mode from the body is much stronger than that from the edge, which makes it extremely hard to collect signal purely from the edges. This is also one of our motivations to employ Raman mapping which is able to provide more statistical data. This material is available free of charge *via* the Internet at http://pubs.acs.org.

REFERENCES AND NOTES

1. Novoselov, K. S.; Geim, A. K.; Morozov, S. V.; Jiang, D.; Zhang, Y.; Dubonos, S. V.; Grigorieva, I. V.; Firsov, A. A. Electric Field Effect in Atomically Thin Carbon Films. *Science* **2004**, *306*, 666–669.
2. Geim, A. K.; Novoselov, K. S. The Rise of Graphene. *Nat. Mater.* **2007**, *6*, 183–191.
3. Zhang, Y.; Tan, Y. W.; Stormer, H. L.; Kim, P. Experimental Observation of the Quantum Hall Effect and Berry's Phase in Graphene. *Nature* **2005**, *438*, 201–204.
4. Nakada, K.; Fujita, M.; Dresselhaus, G.; Dresselhaus, M. S. Edge State in Graphene Ribbons: Nanometer Size Effect and Edge Shape Dependence. *Phys. Rev. B* **1996**, *54*, 17954–17961.
5. Sasaki, K.; Sato, K.; Saito, R.; Jiang, J. Local Density of States at Zigzag Edges of Carbon Nanotubes and Graphene. *Phys. Rev. B* **2007**, *75*, 235430-1–235430-7.
6. Sasaki, K.; Jiang, J.; Saito, R.; Onari, S.; Tanaka, Y. J. Theory of Superconductivity of Carbon Nanotubes and Graphene. *Phys. Soc. Jpn.* **2007**, *76*, 033702-1–033702-4.
7. Abanin, D. A.; Lee, P. A.; Levitov, L. S. Charge and Spin Transport at the Quantum Hall Edge of Graphene. *Solid State Commun.* **2007**, *143*, 77–85.
8. Cervantes, F.; Piscanec, S.; Csanyi, G.; Ferrari, A. C. Edge-Functionalized and Substitutionally Doped Graphene Nanoribbons: Electronic and Spin Properties. *Phys. Rev. B* **2008**, *77*, 165427-1–165427-13.
9. Thomsen, C.; Reich, S. Double Resonant Raman Scattering in Graphite. *Phys. Rev. Lett.* **2000**, *85*, 5214–5217.
10. Ferrari, A. C.; Robertson, J. Interpretation of Raman Spectra of Disordered and Amorphous Carbon. *Phys. Rev. B* **2000**, *61*, 14095–14107.
11. Ferrari, A. C.; Meyer, J. C.; Scardaci, V.; Casiraghi, C.; Lazzeri, M.; Mauri, F.; Piscanec, S.; Jiang, D.; Novoselov, K. S.; Roth, S.; *et al.* Raman Spectrum of Graphene and Graphene Layers. *Phys. Rev. Lett.* **2006**, *97*, 187401-1–187401-4.
12. Ni, Z. H.; Wang, H. M.; Kasim, J.; Fan, H. M.; Yu, T.; Wu, Y. H.; Feng, Y. P.; Shen, Z. X. Graphene Thickness Determination Using Reflection and Contrast Spectroscopy. *Nano Lett.* **2007**, *7*, 2758–2763.
13. Mafra, D. L.; Samsonidze, G.; Malard, L. M.; Elias, D. C.; Brant, J. C.; Plentz, F.; Alves, E. S.; Pimenta, M. A. Determination of LA and TO Phonon Dispersion Relations of Graphene near the Dirac Point by Double Resonance Raman Scattering. *Phys. Rev. B* **2007**, *76*, 233407-1–233407-4.
14. Huang, M.; Yan, H.; Chen, C.; Song, D.; Heinz, T. F.; Hone, J. Phonon Softening and Crystallographic Orientation of Strained Graphene Studied by Raman Spectroscopy. *Proc. Natl. Acad. Sci. U.S.A.* **2009**, *106*, 7304–7308.
15. Mohiuddin, T. M. G.; Lombardo, A.; Nair, R. R.; Bonetti, A.; Savini, G.; Jalil, R.; Bonini, N.; Basko, D. M.; Galiotis, C.; Marzari, N.; *et al.* Uniaxial Strain in Graphene by Raman Spectroscopy: G Peak Splitting, Grüneisen Parameters, and Sample Orientation. *Phys. Rev. B* **2007**, *79*, 205433-1–205433-8.
16. Das, A.; Pisana, S.; Chakraborty, B.; Piscanec, S.; Saha, S. K.; Waghmare, U. V.; Novoselov, K. S.; Krishnamurthy, H. R.; Geim, A. K.; Ferrari, A. C.; *et al.* Monitoring Dopants by Raman Scattering in an Electrochemically Top-Gated Graphene Transistor. *Nat. Nanotechnol.* **2008**, *3*, 210–215.
17. Luo, Z.; Yu, T,; Kim, K; Ni, Z.; You, Y.; Lim, S.; Shen, Z.; Wang, S.; Lin, J. Thickness-Dependent Reversible Hydrogenation of Graphene Layers. *ACS Nano* **2009**, *3*, 1781–1788.
18. Cancado, L. G.; Pimenta, M. A.; Saito, R.; Jorio, A.; Ladeira, L. O.; Grueneis, A.; Souza-Filho, A. G.; Dresselhaus, G.; Dresselhaus, M. S. Stokes and Anti-Stokes Double Resonance Raman Scattering in Two-Dimensional Graphite. *Phys. Rev. B* **2002**, *66*, 035415-1–035415-5.
19. Yu, T.; Ni, Z.; Du, C.; You, Y.; Wang, Y.; Shen, Z. Raman Mapping Investigation of Graphene on Transparent Flexible Substrate: The Strain Effect. *J. Phys. Chem. C* **2008**, *112*, 12602–12605.
20. Ni, Z. H.; Yu, T.; Lu, Y. H.; Wang, Y. Y.; Feng, Y. P.; Shen, Z. X. Uniaxial Strain on Graphene: Raman Spectroscopy Study and Band-Gap Opening. *ACS Nano* **2008**, *2*, 2301–2305.
21. You, Y. M.; Ni, Z. H.; Yu, T.; Shen, Z. X. Edge Chirality Determination of Graphene by Raman Spectroscopy. *Appl. Phys. Lett.* **2008**, *93*, 163112-1–163112-3.
22. Cancado, L. G.; Pimenta, M. A.; Neves, B. R. A.; Dantas,

M. S. S.; Jorio, A. Influence of the Atomic Structure on the Raman Spectra of Graphite Edges. *Phys. Rev. Lett.* **2004**, *93*, 247401-1–247401-4.
23. Gupta, A. K.; Russin, T. J.; Gutiérrez, H. R.; Eklund, P. C. Probing Graphene Edges *via* Raman Scattering. *ACS Nano* **2009**, *3*, 45–52.
24. Casiraghi, C.; Hartschuh, A.; Qian, H.; Piscanec, S.; Georgi, C.; Fasoli, A.; Novoselov, K. S.; Basko, D. M.; Ferrari, A. C. Raman Spectroscopy of Graphene Edges. *Nano Lett.* **2009**, *9*, 1433–1441.
25. Sasaki, K.; Saito, R.; Wakabayashi, K.; Enoki, T. Identifying the Orientation of Edge of Graphene Using G Band Raman Spectra. *J. Phys. Soc. Jpn.* **2010**, *79*, 044603-1–044603-8.
26. Loudon, R. The Raman Effect in Crystals. *Adv. Phys.* **1964**, *13*, 423–482.
27. Yoon, D.; Moon, H.; Son, Y. W.; Samsonidze, G.; Park, B. H.; Kim, J. B.; Lee, Y. P.; Cheong, H. Strong Polarization Dependence of Double-Resonant Raman Intensities in Graphene. *Nano Lett.* **2008**, *8*, 4270–4274.
28. Tsoukleri, G.; Parthenios, J.; Papagelis, K.; Jalil, R.; Ferrari, A. C.; Geim, A. K.; Novoselov, K. S.; Galiotis, C. Subjecting a Graphene Monolayer to Tension and Compression. *Small* **2009**, *5*, 2397–2402.
29. Sasaki, K.; Yamamoto, M.; Murakami, S.; Saito, R.; Dresselhaus, M. S.; Takai, K; Mori, T.; Enoki, T.; Wakabayashi, K. Kohn Anomalies in Graphene Nanoribbons. *Phys. Rev. B* **2009**, *80*, 155450-1–155450-11.